

SiMaN: Sign-to-Magnitude Network Binarization

Mingbao Lin, Rongrong Ji, *Senior Member, IEEE*, Zihan Xu, Baochang Zhang, *Senior Member, IEEE*, Fei Chao, *Member, IEEE*, Mingliang Xu, Chia-Wen Lin *Fellow, IEEE* and Ling Shao, *Fellow, IEEE*

Abstract—Binary neural networks (BNNs) have attracted broad research interest due to their efficient storage and computational ability. Nevertheless, a significant challenge of BNNs lies in handling discrete constraints while ensuring bit entropy maximization, which typically makes their weight optimization very difficult. Existing methods relax the learning using the sign function, which simply encodes positive weights into +1s, and −1s otherwise. Alternatively, we formulate an angle alignment objective to constrain the weight binarization to $\{0, +1\}$ to solve the challenge. In this paper, we show that our weight binarization provides an analytical solution by encoding high-magnitude weights into +1s, and 0s otherwise. Therefore, a high-quality discrete solution is established in a computationally efficient manner without the sign function. We prove that the learned weights of binarized networks roughly follow a Laplacian distribution that does not allow entropy maximization, and further demonstrate that it can be effectively solved by simply removing the ℓ_2 regularization during network training. Our method, dubbed sign-to-magnitude network binarization (SiMaN), is evaluated on CIFAR-10 and ImageNet, demonstrating its superiority over the sign-based state-of-the-arts. Our source code, experimental settings, training logs and binary models are available at <https://github.com/lmbxmu/SiMaN>.

Index Terms—Binary neural network, Network binarization, weight magnitude, angular alignment, network compression & acceleration, network quantization.

1 INTRODUCTION

DEEP neural networks (DNNs), especially convolutional neural networks (CNNs), have been effectively used in many tasks of computer vision, such as image recognition [1], [2], [3], object detection [4], [5], [6], and semantic segmentation [7], [8], [9]. Nowadays, DNNs are almost trained on high-capacity but power-hungry graphics processing units (GPUs); however, such DNN models often fail to run on low-power devices such as cell phones and Internet-of-Things (IoT) devices. As a result, substantial efforts have been invested to reduce the model redundancy with a comparable or even better performance in comparison with the full model, such that the compressed model can be easily run on resource-limited devices.

Typical methods for reducing the model redundancy include, but are not limited to: (1) Weight pruning discards individual weights in the filters or connections across different layers, and then reshapes the model in a sparse format [10], [11]. (2) Filter pruning resorts to directly removing a whole filter and its corresponding channel in the next layer [12], [13]. (3) Compact networks, such as ShuffleNets [14], [15], MobileNets [16], [17], [18] and GhostNet [19], directly design parameter-efficient neural network models. (4) Tensor

decomposition approximates the weight tensor with a series of low-rank matrices, which are then organized in a sum-product form [20], [21]. (5) Low-precision quantization aims to compress the model by reducing the number of bits used to represent the weight parameters of the pre-trained models [22], [23], [24].

In particular, binary neural networks (BNNs), which quantize their weights and activations in a 1-bit binary form, have attracted increasing attention for two major reasons: 1) The memory usage of a BNN is $32\times$ lower than its full-precision counterpart, since the weights of the latter are stored in a 32-bit floating-point form. 2) A significant reduction of computational complexity can be achieved by executing efficient XNOR and bitcount operations, *e.g.*, up to $58\times$ speed-ups on CPUs as reported by [25]. Nevertheless, BNNs are also famed for their significant performance degradation. For example, XNOR-Net [25] suffers an 18% drop in top-1 accuracy when binarizing ResNet-18 on the ImageNet classification task [26]. This greatly restricts the deployment of BNNs.

One of the major obstacles in constructing a high-performing BNN is the discrete constraints imposed on the pursued binary weights, which challenges the weight optimization. Meanwhile, BNNs also require the two possible values of binarized weights to be uniformly (half-half) distributed to ensure bit entropy maximization. To this end, most existing approaches simply employ the sign function to binarize weights where positive weights are encoded into +1s, and −1s are used otherwise [24], [25], [27], [28], [29]. To compensate for the entropy information, recent methods, such as Bayesian optimization [30], rotation matrix [24], and weight standardization [29], learn a two-mode distribution for real-valued weights to increase the probability of encoding one half of the weights into +1s and the other half into −1s by the sign function. These strategies, however, increase the learning complexity, since

- M. Lin, R. Ji (Corresponding Author), Z. Xu and F. Chao are with the Media Analytics and Computing Laboratory, Department of Artificial Intelligence, School of Informatics, Xiamen University, Xiamen 361005, China (e-mail: rjji@xmu.edu.cn).
- B. Zhang is with the School of Automation Science and Electrical Engineering, Beihang University, China.
- M. Xu is with the Tencent Youtu Lab, Shanghai 200233, China
- C.-W. Lin is with the Department of Electrical Engineering and the Institute of Communications Engineering, National Tsing Hua University, Hsinchu 30013, Taiwan.
- L. Shao is with the Inception Institute of Artificial Intelligence, Abu Dhabi, United Arab Emirates, and also with the Mohamed bin Zayed University of Artificial Intelligence, Abu Dhabi, United Arab Emirates.

Manuscript received April 19, 2005; revised August 26, 2015.

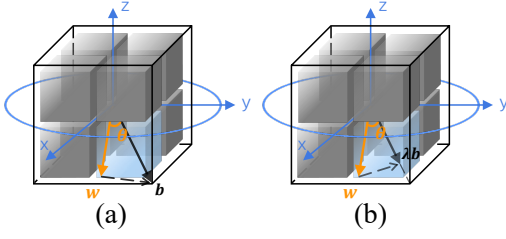


Fig. 1. (a) Early works [31], [32] suffer from large quantization error caused by both the norm gap and angular bias between the full-precision weights and its binarized version. (b) Recent works [25], [29] introduce a scaling factor to reduce the norm gap but cannot reduce the angular bias, i.e., θ . Therefore the quantization error $\|\mathbf{w} \sin \theta\|^2$ is still large when θ is large.

the optimization involves additional training loss terms and variables. Moreover, it is unclear whether the simple usage of the sign function is the optimal encoding option for the weight binarization process.

Another obstacle in learning BNNs comes at the large quantization error between the full-precision weight vector \mathbf{w} and its binary vector \mathbf{b} [31], [32] as shown in Fig. 1(a). To solve this, state-of-the-art approaches [25], [29] try to lessen the quantization error by introducing a per-channel learnable/optimizable scaling factor λ to minimize the quantization error

$$\min_{\lambda, \mathbf{b}} \|\lambda \mathbf{b} - \mathbf{w}\|^2. \quad (1)$$

However, as revealed in the previous work [24], the introduction of λ only partly mitigates the quantization error by compensating for the norm gap between the full-precision weight and its binarized version, but cannot reduce the quantization error due to an angular bias as shown in Fig. 1(b). Apparently, with a fixed angular bias θ , when $\lambda \mathbf{b} - \mathbf{w}$ is orthogonal to $\lambda \mathbf{b}$, Eq. (1) reaches the minimum and we have

$$\|\mathbf{w} \sin \theta\|^2 \leq \|\lambda \mathbf{b} - \mathbf{w}\|^2. \quad (2)$$

Thus, $\|\mathbf{w} \sin \theta\|^2$ serves as the lower bound of the quantization error and cannot be diminished as long as the angular bias exists. This lower bound could be huge with a large angular bias θ . Thus, it is desirable to reduce this angular error for the sake of further reducing the quantization error.

To solve the angular bias, Lin *et al* [24] proposed the angle alignment based learning objective, which is originally formulated as

$$\arg \max_{\mathbf{R}} \frac{\text{sign}(\mathbf{R}^T \mathbf{w})^T (\mathbf{R}^T \mathbf{w})}{\|\text{sign}(\mathbf{R}^T \mathbf{w})\|_2 \|\mathbf{R}^T \mathbf{w}\|_2}, \quad (3)$$

$$\text{s.t. } \mathbf{R}^T \mathbf{R} = \mathbf{I}_n,$$

where \mathbf{R} is constrained to an n -order rotation matrix. As shown in Fig. 2(a), by applying the sign function on the rotated weight vector $\mathbf{R}^T \mathbf{w}$, we attain the binarization of \mathbf{w} , i.e., $\mathbf{b}_w \in \text{sign}(\mathbf{R}^T \mathbf{w})$. Thus, Eq. (3) aims to learn a rotation matrix such that the angle bias between the rotated weight vector and its encoded binarization is reduced by the sign function. However, the learning complexity of the rotation matrix, \mathbf{R} , is very high, due to the non-convexity of Eq. (3). Thus, an alternating optimization approach is developed,

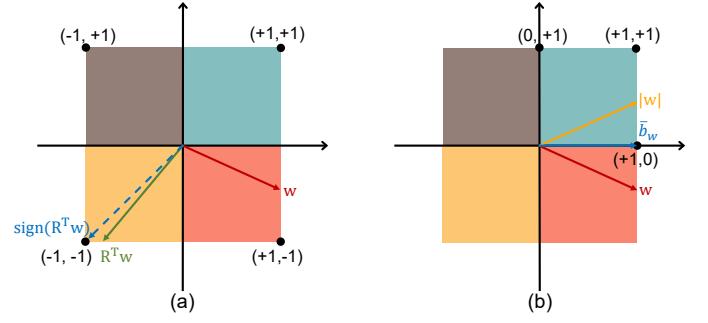


Fig. 2. Comparison between (a) RBNN [24] and (b) our SiMaN. RBNN learns a rotation matrix \mathbf{R} first, and then applies the sign function to binarize the rotated weight $\mathbf{b}_w = \text{sign}(\mathbf{R}^T \mathbf{w}) \in \{-1, +1\}^n$. In contrast, ours involves the magnitude of the weight, and then discretely learns $\mathbf{b}_w \in \{0, 1\}^n$.

which however results sub-optimal binarization. Moreover, the optimization is still built upon the sign function.

In this paper, a novel sign-to-magnitude network binarization (SiMaN) is proposed to discretely encode DNNs, leading to improved accuracy. Within our method, we reformulate the recent angle alignment objective [24], which aims to maximize the cosine distance between the full-precision weight vector and its encoded binarization. Different from existing works that binarize weights into $\{-1, +1\}$ by the sign function, our binarization falls into $\{0, +1\}$ as illustrated in Fig. 2(b). In this way, we reveal that the globally analytical binarization for our angle alignment can be found in a computationally efficient manner of $\mathcal{O}(n \log n)$ by quantizing into +1s the high-magnitude weights, and 0s otherwise, therefore enabling weight binarization without the sign function. To the best of our knowledge, we prove for the first time that the learned real-valued weights roughly follow a Laplacian distribution, which results in around 37% of weights being encoded into +1s. This prevents the BNN from maximizing the entropy of information. To solve this, we do not add a term to the loss function since this increases the optimization difficulty. Alternatively, we analyze the intrinsic numerical values of weights, and show that the simple removal of the ℓ_2 regularization destroys the Laplacian distribution, and thus enhances the half-half weight binarization. As a result, the final binarization is obtained by encoding into +1s weights within the largest top-half magnitude, and 0s otherwise to further reduce the computational complexity from $\mathcal{O}(n \log n)$ to $\mathcal{O}(n)$.

In summary, the main contributions we have made in this paper are listed in the following.

- A new learning objective based on the angle alignment is proposed and a magnitude-based analytical solution is developed in a computationally efficient manner.
- We formally prove that the learned weights in BNNs follow a Laplacian distribution, which, as revealed, prevents the maximization of bit entropy.
- A detailed analysis on the numerical values of weights shows that simply removing the ℓ_2 regularization benefits maximizing the bit entropy while further reducing the computational complexity.

- Experiments on CIFAR-10 [33] and ImageNet [26] demonstrate that our sign-to-magnitude framework for network binarization outperforms the traditional sign-based binarization.

2 RELATED WORK

Following the introduction of pioneering research [32] where the sign function and the straight-through estimator (STE) [34] are respectively adopted for the forward weight/activation binarization and backward gradient updating, BNNs have emerged as one of the most appealing approaches for the deployment of DNNs in resource-limited devices. As such, great efforts have been put into closing the gap between full-precision networks and their BNNs. In what follows, we briefly review some related works. A comprehensive overview can be found in the survey papers [35], [36].

XNOR-Net [25] introduces two scaling factors for channel-wise weights and activations to minimize quantization error. Inspired by this, XNOR-Net++ [37] improves the performance by integrating the two scaling factors into one, which is then updated using the standard gradient propagation. Except for the scaling factors, RBNN [24] further reduces the quantization error by optimizing the angle difference between a full-precision weight vector and its binarization. To enable the gradient propagation and reduce the “gradient mismatch” by the STE [34], several works, such as the swish function [38], piece-wise polynomial function [28], and error decay estimator [29], formulate the forward/backward quantization as a differentiable non-linear mapping.

Another direction circumvents the gradient approximation of the sign function by sampling from the weight distribution [39], [40]. There are also abundant works that explore the optimization of BNNs [41], [42], [43], [44], [45] and explain their effectiveness [46]. Recent works [38], [47] embed various regularization terms into the training loss to binarize the weights and control the activation ranges [48]. Moreover, other recent studies devise binarization-friendly structures to boost the performance. For example, Bi-Real [28] designs double residual connections with full-precision downsampling layers. XNOR-Net++ [37] replaces ReLU by PReLU. ReActNet [49] adds parameter-free short-cuts on MobileNetV1 [16] and the group convolution is replaced by a regular convolution.

3 BINARY NEURAL NETWORKS

For an L -layer CNN model, we denote $\mathbf{W}^i = \{\mathbf{w}_1^i, \mathbf{w}_2^i, \dots, \mathbf{w}_{c_{out}^i}^i\} \in \mathbb{R}^{n^i \times c_{out}^i}$ as the real-valued weight set for the i -th layer, where $\mathbf{w}_j^i \in \mathbb{R}^{n^i}$ denotes the j -th weight. The real-valued input activations of the i -th layer are represented as $\mathbf{A}^i = \{\mathbf{a}_1^i, \mathbf{a}_2^i, \dots, \mathbf{a}_{c_{in}^i}^i\} \in \mathbb{R}^{m^i \times c_{in}^i}$; here, c_{out}^i and c_{in}^i respectively represent the output and input channels, and n^i and m^i denote the size of each weight and input, respectively. Then, the convolution result is expressed by

$$\mathbf{a}_j^{i+1} = \mathbf{w}_j^i \otimes \mathbf{A}^i, \quad (4)$$

where \otimes stands for the convolution operation. For simplicity, we omit the non-linear layer here.

BNN Training. To train a BNN, the real-valued \mathbf{w}_j^i and \mathbf{A}^i in Eq.(4) are quantized into binary values $(\mathbf{b}_w)_j^i \in \{-1, +1\}^{n^i}$ and $(\mathbf{B}_A)^i \in \{-1, +1\}^{c_{in}^i \times m^i}$, respectively. As a result, the convolution result can be approximated as

$$\mathbf{a}_j^{i+1} \approx \beta_j^i \cdot (\mathbf{b}_w)_j^i \otimes (\mathbf{B}_A)^i, \quad (5)$$

where β_j^i is a channel-level scaling factor [25], [37].

For the implementation of the BNN training, the forward calculation is fulfilled by conducting the convolution between $(\mathbf{b}_w)_j^i$ and $(\mathbf{B}_A)^i$ in Eq. (5), whereas their real-valued counterparts, \mathbf{w}_j^i and \mathbf{A}^i , are updated during backpropagation. To this end, following [24], [37], [50], the activation binarization in this work is simply realized by the sign function,

$$(\mathbf{B}_A)^i = \text{sign}(\mathbf{A}^i) = \begin{cases} +1, & \text{if } \mathbf{A}^i \geq 0, \\ -1, & \text{otherwise.} \end{cases} \quad (6)$$

In the backpropagation phase, we adopt the piece-wise polynomial function [28] to approximate the gradient of a given loss \mathcal{L} w.r.t. the input activations \mathbf{A}^i as follows

$$\frac{\partial \mathcal{L}}{\partial \mathbf{A}^i} = \frac{\partial \mathcal{L}}{\partial (\mathbf{B}_A)^i} \cdot \frac{\partial (\mathbf{B}_A)^i}{\partial (\mathbf{A}^i)} \approx \frac{\partial \mathcal{L}}{\partial (\mathbf{B}_A)^i} \cdot \frac{\partial F(\mathbf{A}^i)}{\partial \mathbf{A}^i}, \quad (7)$$

where $\frac{\partial F(\mathbf{A}^i)}{\partial \mathbf{A}^i}$ is defined by

$$\frac{\partial F(\mathbf{A}^i)}{\partial \mathbf{A}^i} = \begin{cases} 2 + 2\mathbf{A}^i, & \text{if } -1 \leq \mathbf{A}^i < 0, \\ 2 - 2\mathbf{A}^i, & \text{if } 0 \leq \mathbf{A}^i < 1, \\ 0, & \text{otherwise.} \end{cases} \quad (8)$$

Besides, the STE [34] is used to calculate the gradient of the loss \mathcal{L} w.r.t. the weight \mathbf{w}_j^i as

$$\frac{\partial \mathcal{L}}{\partial \mathbf{w}_j^i} = \frac{\partial \mathcal{L}}{\partial (\mathbf{b}_w)_j^i} \cdot \frac{\partial (\mathbf{b}_w)_j^i}{\partial \mathbf{w}_j^i} \approx \frac{\partial \mathcal{L}}{\partial (\mathbf{b}_w)_j^i}. \quad (9)$$

BNN Inference. In practical deployment, the BNN model is accelerated using the efficient XNOR and bit-count logics embedded in the hardware. Thus, the quantized weights and activations need to be further transformed into $\{0, 1\}$ space. Such a transformation can be realized by setting

$$(\bar{\mathbf{B}}_A)^i = (1 + (\mathbf{B}_A)^i)/2. \quad (10)$$

$$(\bar{\mathbf{b}}_w)_j^i = (1 + (\mathbf{b}_w)_j^i)/2. \quad (11)$$

Then, the approximated convolution in Eq.(5) can be replaced by the following equality

$$\mathbf{a}_j^{i+1} \approx \beta_j^i \cdot (2 \cdot (\bar{\mathbf{b}}_w)_j^i \odot (\bar{\mathbf{B}}_A)^i - n^i), \quad (12)$$

where \odot represents the XNOR and bitcount operations that are well-fitted for real-time network inference.

Our Insight. In this paper, we focus on binarizing the real-valued weight \mathbf{w}_j^i . Different from most existing works [24], [37], [50], [51] that project weights \mathbf{w}_j^i into $(\mathbf{b}_w)_j^i \in \{-1, +1\}^{n^i}$ using the sign function during training and then transform $(\mathbf{b}_w)_j^i$ into $(\bar{\mathbf{b}}_w)_j^i \in \{0, +1\}^{n^i}$ for inference, we seek to directly encode the weights into $\bar{\mathbf{b}}_w \in \{0, +1\}^{n^i}$ and then devise an efficient optimization to attain the optimal solution in Sec.4.1. We demonstrate

in Sec. 4.2 that the weight, w_j^i , roughly follows a Laplacian distribution, which inhibits the entropy maximization. We reveal that this can be easily addressed by removing the ℓ_2 regularization in Sec. 4.3.

For simplicity, the scripts “ i ” and “ j ” are omitted in the following context.

4 WEIGHT BINARIZATION

In this section, we specify the formulation of our weight binarization, including the binary learning objective, weight distribution, and bit entropy maximization.

4.1 Learning Objective

To achieve high-quality weight binarization, different from the existing work [24], we reformulate the learning objective in Eq. (3) as

$$\begin{aligned} \arg \max_{\bar{\mathbf{b}}_w} \frac{(\bar{\mathbf{b}}_w)^T |\mathbf{w}|}{\|\bar{\mathbf{b}}_w\|_2 \|\mathbf{w}\|_2}, \\ \text{s.t. } \bar{\mathbf{b}}_w \in \{0, +1\}^n, \end{aligned} \quad (13)$$

where $|\cdot|$ returns the absolute result of its input.

As can be seen, our learning objective is also built on the basis of angle alignment. Nevertheless, our method differs from Eq. (3) in many aspects: First, we drop the sign function since variables in a binarized network must be retained in a discrete set; thus, the binarization should be built upon the concept of the discrete optimization rather than the simple sign function. Second, we encode the weights into $\bar{\mathbf{b}}_w \in \{0, +1\}^n$ rather than $\mathbf{b}_w \in \{-1, +1\}^n$. In Corollary 1, we show that $\bar{\mathbf{b}}_w \in \{0, +1\}^n$ allows us to find an analytical solution in an efficient manner by transferring the high-magnitude weights to +1s and 0s otherwise. Third, our angle alignment is independent of the rotation matrix, \mathbf{R} , since we remove the sign function, which makes the rotation direction unpredictable. Lastly, we align the angle difference between the binarization and absolute weight vector, $|\mathbf{w}|$, instead of the weight \mathbf{w} itself. The rationale behind this is that our binarization falls into the non-negative set $\bar{\mathbf{b}}_w$. Fig. 2(b) outlines our binarization process.

Note that $\|\mathbf{w}\|_2$ is irrelevant to the optimization of Eq. (13). Thus, the learning can be simplified to

$$\begin{aligned} \arg \max_{\bar{\mathbf{b}}_w} \frac{(\bar{\mathbf{b}}_w)^T |\mathbf{w}|}{\|\bar{\mathbf{b}}_w\|_2}, \\ \text{s.t. } \bar{\mathbf{b}}_w \in \{0, +1\}^n. \end{aligned} \quad (14)$$

This is an integer programming problem [52]. Nevertheless, as demonstrated in Corollary 1, by learning the encoding space in $\{0, +1\}^n$, we can reach the global maximum in a substantially efficient fashion.

Corollary 1. For Eq. (14), the computational complexity of finding the global optimum is $\mathcal{O}(n \log n)$.

Proof: For $\bar{\mathbf{b}}_w \in \{0, +1\}^n$, it is intuitive to see that $\|\bar{\mathbf{b}}_w\|_2$ falls into the set $\{\sqrt{1}, \dots, \sqrt{n}\}$. Considering that $\|\bar{\mathbf{b}}_w\|_2 = \sqrt{k}$ ($k = 1, \dots, n$), the integer programming problem in Eq. (14) can be maximized by encoding to +1s those elements of $\bar{\mathbf{b}}_w$ that correspond to the largest k entries of $|\mathbf{w}|$. To this end, we need to perform sorting upon $|\mathbf{w}|$, for which the complexity is $\mathcal{O}(n \log n)$. Since k has n possible

values, we need to evaluate Eq. (14) n times, and then select the $\bar{\mathbf{b}}_w$ that maximizes the objective function, leading to a linear complexity with n . Hence, the overall complexity is $\mathcal{O}(n \log n)$. ■

Therefore, given one filter weight $\mathbf{w} \in \mathbb{R}^n$, we can find the binarization $\bar{\mathbf{b}}_w \in \{0, +1\}^n$ having the smallest angle with $|\mathbf{w}|$. Note that $\bar{\mathbf{b}}_w$ found in this way is the global optimum. Furthermore, we emphasize that the proof of Corollary 1 indicates that the binarization in our framework involves the magnitudes of weights instead of the signs of weights, which significantly differentiates our work from existing works. In the next two sections, we show that the overall complexity can be further reduced to $\mathcal{O}(n)$, given the bit entropy maximization.

4.2 Weight Distribution

The capacity of a binarization model, often measured by the bit entropy, is maximized when it is half-half distributed, *i.e.*, one half of the weights are encoded into 0 and the other half are encoded into +1 [24], [29]. In this case, we expect to maximize our objective in Eq. (14) when those weights with the top-half magnitudes are encoded into +1s and the remaining are encoded into 0s. However, we reveal that it is difficult to binarize \mathbf{w} with entropy maximization due to its specific form of distribution.

Specifically, after training, $w \in \mathbf{w}$ is widely believed to roughly obey a zero-mean Laplacian distribution, *i.e.*, $w \sim \text{La}(0, b)$, or a zero-mean Gaussian distribution, *i.e.*, $w \sim \mathcal{N}(0, \sigma^2)$ [22], [53], [54]. In Corollary 2, for the first time, we demonstrate its specific distribution.

Corollary 2. $w \in \mathbf{w}$ roughly follows a zero-mean Laplacian distribution.

Proof: Suppose w is encoded into +1 if $|w| > t$, and 0 otherwise. Note that the learning of Eq. (14) can also be regarded as a problem of finding the centroid of a subset [55], which can be calculated by the integral:

$$\begin{aligned} \frac{(\bar{\mathbf{b}}_w)^T |\mathbf{w}|}{\|\bar{\mathbf{b}}_w\|_2} &= \frac{\int_{-\infty}^{-t} w f(w) dw + \int_t^{+\infty} w f(w) dw}{\sqrt{\int_{-\infty}^{-t} f(w) dw + \int_t^{+\infty} f(w) dw}} \\ &= \frac{2 \int_t^{+\infty} w f(w) dw}{\sqrt{2 \int_t^{+\infty} f(w) dw}}, \end{aligned} \quad (15)$$

where $f(w)$ denotes the probability density function. Let p_{+1} denote the proportion of \mathbf{w} being encoded into +1s, which can be calculated by

$$p_{+1} = 1 - 2 \int_0^t f(w) dw. \quad (16)$$

Here, we first derive the theoretical values of p_{+1} when $p(w)$ follows a Laplacian or Gaussian distribution, and then experimentally verify our proof.

Laplacian distribution. In this case, we have $f(w) = \frac{1}{2b} e^{-w/b}$. Therefore, Eq. (15) becomes

$$\begin{aligned} \frac{(\bar{\mathbf{b}}_w)^T |\mathbf{w}|}{\|\bar{\mathbf{b}}_w\|_2} &= \frac{2 \int_t^{+\infty} \frac{w}{2b} e^{-w/b} dw}{\sqrt{2 \int_t^{+\infty} \frac{1}{2b} e^{-w/b} dw}} \\ &= \frac{(b+t)e^{-t/b}}{\sqrt{e^{-t/b}}} \\ &= (b+t)\sqrt{e^{-t/b}}. \end{aligned} \quad (17)$$

Setting $\frac{\partial(b+t)\sqrt{e^{-t/b}}}{\partial t} = 0$ to attain the maximum of Eq. (17), we have $t = b$. The proportion of +1s can be obtained as

$$p_{+1} = 1 - 2 \int_0^t \frac{1}{2b} e^{-w/b} dw \approx 0.37. \quad (18)$$

Gaussian distribution. In this case, we have $f(w) = \frac{1}{\sqrt{2\pi}\sigma} e^{-w^2/(2\sigma^2)}$. Similarly, Eq. (15) can be rewritten as

$$\begin{aligned} \frac{(\bar{\mathbf{b}}_w)^T}{\|\bar{\mathbf{b}}_w\|_2} |\mathbf{w}| &= \frac{2 \int_t^{+\infty} \frac{w}{\sqrt{2\pi}\sigma} e^{-w^2/(2\sigma^2)} dw}{\sqrt{2 \int_t^{+\infty} \frac{1}{\sqrt{2\pi}\sigma} e^{-w^2/(2\sigma^2)} dw}} \\ &= \frac{\frac{\sigma}{\sqrt{2\pi}} e^{-t^2/(2\sigma^2)}}{\sqrt{\frac{1}{2} \operatorname{erfc}\left(\frac{t}{\sqrt{2}\sigma}\right)}}, \end{aligned} \quad (19)$$

where $\operatorname{erfc}(\cdot)$ denotes the complementary error function.¹

Let $m = \frac{t}{\sqrt{2}\sigma}$, then Eq. (19) can be written as

$$\frac{(\bar{\mathbf{b}}_w)^T}{\|\bar{\mathbf{b}}_w\|_2} |\mathbf{w}| = \frac{\sigma}{\sqrt{\pi}} \frac{e^{-m^2}}{\sqrt{\operatorname{erfc}(m)}}. \quad (20)$$

Setting $\frac{\partial e^{-m^2}/\sqrt{\operatorname{erfc}(m)}}{\partial m} = 0$, we have $m = \frac{t}{\sqrt{2}\sigma} \approx 0.43$. Thus, we obtain $t \approx 0.43\sqrt{2}\sigma$, and then derive the proportion of +1s:

$$p_{+1} = 1 - 2 \int_0^t \frac{1}{\sqrt{2\pi}\sigma} e^{-w^2/(2\sigma^2)} dw \approx 0.54. \quad (21)$$

As mentioned above, the trained weight $w \in \mathbf{w}$ obeys either a Laplacian distribution (with $p_{+1} \approx 0.37$) or a Gaussian distribution (with $p_{+1} \approx 0.54$). In Fig. 3(a), we conduct an experiment which shows a practical p_{+1} of around 0.36 after training.² This implies that $w \in \mathbf{w}$ follows a Laplacian distribution, and our proof is completed. ■

4.3 Maximizing Bit Entropy

The proof of Corollary 1 indicates that the binarization in our framework is related to the weight magnitude, i.e., $|\mathbf{w}|$. However, the Laplacian distribution contradicts the entropy maximization. To solve this, one naive solution is to assign the top half of elements of the sorted $|\mathbf{w}|$ with +1 and assign the remaining elements with 0, that is

$$\tilde{\mathbf{b}}_w = \begin{cases} +1, & \text{top half of sorted } |\mathbf{w}|, \\ 0, & \text{otherwise.} \end{cases} \quad (22)$$

Despite helping achieve entropy maximization, such a simple operation violates the learning objective of minimizing the angular bias in Eq. (14) since \mathbf{b}_w deviates significantly from the optimal $\bar{\mathbf{b}}_w$ as revealed in Corollary 3.

Corollary 3. Suppose $\bar{\mathbf{b}}_w$ is a binarized vector with a total of k +1s and the binarized vector $\tilde{\mathbf{b}}_w$ has r different bits from $\bar{\mathbf{b}}_w$. Then the angle between $\bar{\mathbf{b}}_w$ and $\tilde{\mathbf{b}}_w$ is bounded by $[\arccos \sqrt{\frac{k}{k+r}}, \arccos \sqrt{\frac{k-r}{k}}]$.

Proof: To find the lower bound, we need to obtain $\tilde{\mathbf{b}}_w$ such that $\frac{(\bar{\mathbf{b}}_w)^T \tilde{\mathbf{b}}_w}{\|\bar{\mathbf{b}}_w\|_2 \|\tilde{\mathbf{b}}_w\|_2}$ is maximized. Intuitively, this can be achieved when \mathbf{b}_w has all ones at the same positions as $\bar{\mathbf{b}}_w$,

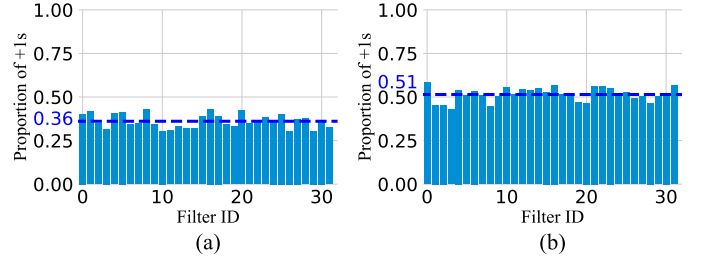


Fig. 3. Proportion of +1s trained (a) with and (b) without the ℓ_2 regularization (Layer2.1.2 of ResNet-20). The dashed blue lines denote the average proportions of +1s of all filter weights.

and r additional ones in the remaining positions, in which $\|\tilde{\mathbf{b}}_w\|_2 = \sqrt{k+r}$ and $(\bar{\mathbf{b}}_w)^T \tilde{\mathbf{b}}_w = k$. Then, we have the lower bound of $\arccos \sqrt{\frac{k}{k+r}}$. To obtain the upper bound, we need to minimize $\frac{(\bar{\mathbf{b}}_w)^T \tilde{\mathbf{b}}_w}{\|\bar{\mathbf{b}}_w\|_2 \|\tilde{\mathbf{b}}_w\|_2}$, which can be done when there are $(k-r)$ +1s in \mathbf{b}_w in the common positions with $\bar{\mathbf{b}}_w$ and the rest are set to zeros. In this case, we have $\|\tilde{\mathbf{b}}_w\|_2 = \sqrt{k-r}$ and $(\bar{\mathbf{b}}_w)^T \tilde{\mathbf{b}}_w = k-r$, which leads to the upper bound of $\arccos \sqrt{\frac{k-r}{k}}$.

According to Corollary 2 and Eq. (22), we have $k \approx 0.37n$, and $r \approx 0.13n$. Then, we can derive the practical angle bounds as $[\arccos \sqrt{\frac{0.37}{0.37+0.13}}, \arccos \sqrt{\frac{0.37-0.13}{0.37}}] \approx [30.66^\circ, 36.35^\circ]$. Therefore, a large angle bias occurs between the solution \mathbf{b}_w from Eq. (22) and the solution $\bar{\mathbf{b}}_w$ from optimizing Eq. (14). In Sec. 5.2, we demonstrate the poor performance when simply using $\tilde{\mathbf{b}}_w$.

Instead of imposing an additional loss term to regularize the ideal half-half binarization, we analyze the numerical value of each weight and reveal that simply removing the ℓ_2 regularization can explicitly maximize the bit capacity, leading to a more informative binarized network.

Let $\mathcal{L}_{\mathbf{b}_w}^k = \arg \max_{\mathbf{b}_w} \frac{(\mathbf{b}_w)^T}{\sqrt{k}} |\mathbf{w}| = \frac{\sum_{i=1}^k \tilde{w}_i}{\sqrt{k}}$ denote the maximum result of the integer programming problem in Eq. (14), where $\tilde{w}_i \in |\mathbf{w}|$ corresponds to the i -th largest magnitude. We have $\mathcal{L}_{\mathbf{b}_w}^{k+1} < \mathcal{L}_{\mathbf{b}_w}^k$, i.e.,

$$\frac{\tilde{w}_{k+1} + \sum_{i=1}^k \tilde{w}_i}{(\sqrt{k+1} - \sqrt{k}) + \sqrt{k}} < \frac{\sum_{i=1}^k \tilde{w}_i}{\sqrt{k}}. \quad (23)$$

We can deduce that

$$\tilde{w}_{k+1} < \mathcal{L}_{\mathbf{b}_w}^k (\sqrt{k+1} - \sqrt{k}). \quad (24)$$

For Laplacian distributed weights, we know that $k \approx 0.37n$. Thus, the above inequality can be rewritten as

$$\tilde{w}_{k+1} < \mathcal{L}_{\mathbf{b}_w}^k (\sqrt{0.37n+1} - \sqrt{0.37n}). \quad (25)$$

Since n is typically thousands for a neural network and we statistically find that $\mathcal{L}_{\mathbf{b}_w}^k$ ranges from 0.63 to 0.73, the multiplication of the two terms in Eq. (25) thus results in an extremely small \tilde{w}_{k+1} approximating to zero. Thus, we need to enlarge the value of \tilde{w}_{k+1} to break the above inequality. We realize that one of the major causes for a small \tilde{w}_{k+1} lies in the existence of the ℓ_2 regularization imposed on the training of neural network. This inspires us to remove the ℓ_2 regularization for the to-be-binarized weights \mathbf{w} .

1. https://en.wikipedia.org/wiki/Error_function.

2. Similar phenomena can be observed in other layers and networks as well (see the supplementary material).

As shown in Fig.3(b), the removal of the ℓ_2 regularization increases the proportion of +1s in $\tilde{\mathbf{b}}_w$ to around 51%. We then further enforce the ideal half-half binarization $\tilde{\mathbf{b}}_w$ using Eq. (22). As a result, $k \approx 0.51n$ and $r \approx 0.01n$, yielding the much smaller angle bounds of $[\arccos \sqrt{\frac{0.51}{0.51+0.01}}, \arccos \sqrt{\frac{0.51-0.01}{0.51}}] \approx [7.97^\circ, 8.05^\circ]$ between $\tilde{\mathbf{b}}_w$ and \mathbf{b}_w . This effectively increases the bit entropy and leads to a nearly optimal solution for the learning objective of Eq. (14). Besides, the half-half binarization further reduces the computational complexity of $\mathcal{O}(n \log n)$ to $\mathcal{O}(n)$ since we only need to find the median of $|\mathbf{w}|$, and encode weights into +1s when their magnitude is larger than the median, and 0s otherwise.

The forward and backward processes of SiMaN are summarized in Algorithm 1. During training, we remove the ℓ_2 regularization and adopt the binarization $\mathbf{b}_w \in \{-1, +1\}^n$ transformed from the half-half binarization $\tilde{\mathbf{b}}_w \in \{0, +1\}^n$ for the convolution in Eq. (5). After training, we obtain a network consisting of a binarized weight \mathbf{b}_w for practical deployment on hardware where the convolution is executed using the XNOR and bitcount operations in Eq. (12).

5 EXPERIMENTS

To demonstrate the efficacy of the proposed SiMaN binarization scheme, we compare its performance with several state-of-the-art BNNs [22], [23], [24], [25], [27], [28], [29], [30], [32], [47], [48], [51], [56], [57], [58], [59] on two image classification datasets, including CIFAR-10 [33] and ImageNet [26].

5.1 Datasets and Experimental Settings

CIFAR-10 [33] consists of 60,000 32×32 images from 10 classes. Each class has 6,000 images. We split the dataset into 50,000 training images and 10,000 testing images. Data augmentation includes random cropping and random flipping, as done in [1] for the training images.

ImageNet [26] contains over 1.2 million images for training and 50,000 validation images from 1,000 classes for classification. Following the recent advances in [23], [24], [29], the data augmentation includes random cropping and flipping.

Network Structures For CIFAR-10, we binarize ResNet-18/20 [1] and VGG-small [60]. For ImageNet, ResNet-18/34 are chosen for binarization. Following [23], [24], [29], double skip connections [28] are added to the ResNets and we do not binarize the first and last layers for all networks.

Implementation Details We implement our SiMaN using Pytorch [61] and all experiments are conducted on NVIDIA Tesla V100 GPUs. We use the cosine scheduler with a learning rate of 0.1 [24], [29]. The SGD is adopted as the optimizer with a momentum of 0.9. For those layers that are not binarized, the weight decay is set to 5×10^{-4} on CIFAR-10 and 1×10^{-4} on ImageNet, and 0 otherwise to remove the ℓ_2 regularization for the bit entropy maximization as discussed in Sec. 4.3. We train the models from scratch with 400 epochs and a batch size of 256 on CIFAR-10, and with 150 epochs and a batch size of 512 on ImageNet.

Note that, we only apply the classification loss during network training for fair comparison. Other training losses such as those proposed in [48], [62], [63], the variants of

Algorithm 1 Sign-to-Magnitude Network Binarization

Input: An L -layer full-precision network with weights $\mathbf{W}^i = \{\mathbf{w}_1^i, \mathbf{w}_2^i, \dots, \mathbf{w}_{c_{out}^i}^i\}$ ($i = 1, 2, \dots, L$), input images (activations) $\mathbf{A}^1 = \{\mathbf{a}_1^1, \mathbf{a}_2^1, \dots, \mathbf{a}_{c_{in}^1}^1\}$.

1) Forward Propagation:

Remove the ℓ_2 regularization term.

for $i = 1$ **to** L **do**

 Binarize the inputs $(\mathbf{B}_A)^i = \text{sign}(\mathbf{A}^i)$ (Eq. (6));

for $j = 1$ **to** c_{out}^i **do**

 Obtain the half-half binarization $(\tilde{\mathbf{b}}_w)_j^i$ (Eq. (22));

 Obtain the binarization $(\mathbf{b}_w)_j^i = 2 \cdot (\tilde{\mathbf{b}}_w)_j^i - 1$ (the inverse of Eq. (11));

 Conduct the convolution $\mathbf{a}_j^{i+1} \approx \beta_j^i \cdot (\mathbf{b}_w)_j^i \otimes (\mathbf{B}_A)^i$ (Eq. (5));

end for

$\mathbf{A}^{i+1} = \{\mathbf{a}_1^{i+1}, \mathbf{a}_2^{i+1}, \dots, \mathbf{a}_{c_{out}^{i+1}}^{i+1}\};$

end for

2) Backward Propagation:

for $i = L$ **to** 1 **do**

 Compute gradient $\frac{\partial \mathcal{L}}{\partial \mathbf{A}^i} \approx \frac{\partial \mathcal{L}}{\partial (\mathbf{B}_A)^i} \cdot \frac{\partial F(\mathbf{A}^i)}{\partial \mathbf{A}^i}$ (Eq. (7));

for $j = 1$ **to** c_{out}^i **do**

 Compute gradient $\frac{\partial \mathcal{L}}{\partial \mathbf{w}_j^i} \approx \frac{\partial \mathcal{L}}{\partial (\mathbf{b}_w)_j^i}$ (Eq. (9));

end for

end for

3) Weight Updating:

for $i = L$ **to** 1 **do**

for $j = 1$ **to** c_{out}^i **do**

 Update $\mathbf{w}_j^i = \mathbf{w}_j^i - \eta \frac{\partial \mathcal{L}}{\partial \mathbf{w}_j^i}$; # η denotes learning rate

end for

end for

Output: An L -layer binarized network with weights $(\tilde{\mathbf{b}}_w)^i = \{(\tilde{\mathbf{b}}_w)_1^i, (\tilde{\mathbf{b}}_w)_2^i, \dots, (\tilde{\mathbf{b}}_w)_{c_{out}^i}^i\} (i = 1, 2, \dots, L)$.

TABLE 1
Ablation studies with/without the ℓ_2 regularization and half-half binarization (ResNet-18 on ImageNet).

| | ℓ_2 regularization | half-half | Top-1(%) | Top-5(%) |
|--------------------|-------------------------|-----------|----------|----------|
| SiMaN ₁ | ✓ | ✗ | 55.1 | 75.5 |
| SiMaN ₂ | ✗ | ✗ | 57.3 | 77.4 |
| SiMaN ₃ | ✓ | ✓ | 59.2 | 81.5 |
| SiMaN | ✗ | ✓ | 60.1 | 82.3 |

network structures in [49], [64], [65], and even the two-step training strategy [45] can be integrated to further boost the binarized networks' performance. These, however, are not considered here. We aim to show the advantages of our magnitude-based optimization solution over the traditional sign-based methods under regular training loss, the same network structure and a common training strategy.

5.2 Ablation Studies

Our SiMaN is built by removing the ℓ_2 regularization and enforcing the half-half strategy in Eq. (22). To analyze their influence, in Table 1, we develop three variants, including (1) SiMaN₁: The ℓ_2 regularization is added while removing the half-half binarization. This variant simply implements binarization based on the proof process of Corollary 1.

TABLE 2

Comparison with the state-of-the-arts on CIFAR-10. W/A denotes the bit length of the weights and activations. Top-1 accuracy is reported.

| Network | Method | W/A | Top-1 (%) |
|-----------|---------------------|-------|-------------|
| ResNet-18 | Full-precision | 32/32 | 94.8 |
| | RAD [48] | 1/1 | 90.5 |
| | IR-Net [29] | 1/1 | 91.5 |
| | RBNN [24] | 1/1 | 92.2 |
| | SiMaN (Ours) | 1/1 | 92.5 |
| ResNet-20 | Full-precision | 32/32 | 92.1 |
| | DoReFa [51] | 1/1 | 79.3 |
| | DSQ [57] | 1/1 | 84.1 |
| | SLB [58] | 1/1 | 85.5 |
| | LNS [23] | 1/1 | 85.8 |
| | IR-Net [29] | 1/1 | 86.5 |
| | SiMaN (Ours) | 1/1 | 87.4 |
| VGG-small | Full-precision | 32/32 | 94.1 |
| | XNOR-Net [25] | 1/1 | 89.8 |
| | BNN [32] | 1/1 | 89.9 |
| | DoReFa [51] | 1/1 | 90.2 |
| | RAD [48] | 1/1 | 90.0 |
| | DSQ [57] | 1/1 | 91.7 |
| | IR-Net [29] | 1/1 | 90.4 |
| | RBNN [24] | 1/1 | 91.3 |
| | SLB [58] | 1/1 | 92.0 |
| | SiMaN (Ours) | 1/1 | 92.5 |

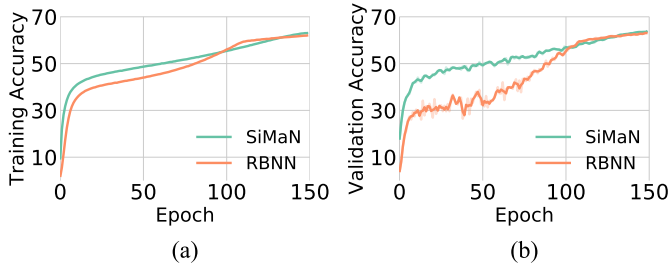


Fig. 4. Comparison of training and validation accuracy curves between our SiMaN and RBNN (ResNet-34 on ImageNet).

It results in around 37% of weights encoded into +1s, as analyzed in Corollary 2, which fails to maximize the entropy information, and thus leads to poorer accuracies of 55.1% for the top-1 and 75.5% for the top-5. (2) SiMaN₂: Both the ℓ_2 regularization and the half-half binarization are removed. It shows better top-1 (57.3%) and top-5 (77.4%) accuracies since the removal of the ℓ_2 regularization breaks the Laplacian distribution and results in around 51% of weights being encoded into +1s as experimentally verified in Fig. 3. (3) SiMaN₃: Both the ℓ_2 regularization and the half-half binarization are added. Though the performance increases, it is still limited. This is because, the half-half binarization with the ℓ_2 regularization causes a large angle deviation of around $30.66^\circ - 36.35^\circ$ as analyzed in Sec. 4.3, from the optimal binarization of our learning objective in Eq. (14).

Based on SiMaN₃, our SiMaN further removes the ℓ_2 regularization. On one hand, this ensures the maximal bit entropy; on the other hand, it ensures that the half-half binarization closely matches the optimal binarization (only $7.97^\circ - 8.05^\circ$ angle deviation as analyzed in Sec. 4.3), thereby leading to the best performance in Table 1.

TABLE 3

Comparison with the state-of-the-arts on ImageNet. W/A denotes the bit length of the weights and activations. Both top-1 and top-5 accuracies are reported.

| Network | Method | W/A | Top-1 (%) | Top-5 (%) |
|-----------|---------------------|-------|-------------|-------------|
| ResNet-18 | Full-precision | 32/32 | 69.6 | 89.2 |
| | BNN [32] | 1/1 | 42.2 | 67.1 |
| | XNOR-Net [25] | 1/1 | 51.2 | 73.2 |
| | DoReFa [51] | 1/2 | 53.4 | - |
| | HWGQ [22] | 1/2 | 59.6 | 82.2 |
| | TBN [56] | 1/2 | 55.6 | 79.0 |
| | Bi-Real [28] | 1/1 | 56.4 | 79.5 |
| | PDNN [47] | 1/1 | 57.3 | 80.0 |
| | BONN [30] | 1/1 | 59.3 | 81.6 |
| | Si-BNN [59] | 1/1 | 59.7 | 81.8 |
| | IR-Net [29] | 1/1 | 58.1 | 80.0 |
| ResNet-34 | LNS [23] | 1/1 | 59.4 | 81.7 |
| | RBNN [24] | 1/1 | 59.9 | 81.9 |
| | SiMaN (Ours) | 1/1 | 60.1 | 82.3 |
| | Full-precision | 32/32 | 73.3 | 91.3 |
| | ABC-Net [27] | 1/1 | 52.4 | 76.5 |
| ResNet-34 | Bi-Real [28] | 1/1 | 62.2 | 83.9 |
| | IR-Net [29] | 1/1 | 62.9 | 84.1 |
| | RBNN [24] | 1/1 | 63.1 | 84.4 |
| | SiMaN (Ours) | 1/1 | 63.9 | 84.8 |

5.3 Convergence

We first show the convergence ability of our SiMaN, and compare it with another angle alignment-based RBNN, which implements network binarization with the sign function [24]. The experiments in Fig. 4 show that our sign-to-magnitude weight binarization has a significantly better ability to converge during BNN training than the traditional sign-based optimization on both training and validation sets, which demonstrates the feasibility of our discrete solution in learning BNNs.

5.4 Results on CIFAR-10

We first conduct detailed studies on CIFAR-10 for the proposed SiMaN as shown in Table 2. As can be seen, our sign-to-magnitude binarization consistently outperforms the recent sign-based state-of-the-arts. Specifically, SiMaN outperforms RBNN [24], IR-Net [29] and SLB [58] by 0.3%, 0.9% and 0.5% in binarizing ResNet-18, ResNet-20 and VGG-small, respectively. The results emphasize the importance of building discrete optimization to pursue high-quality weight binarization. Importantly, compared with another angle alignment-based method, *i.e.*, RBNN, our SiMaN increases the performance to 92.5% when binarizing VGG-small, leading to a performance gain of 1.2%. Besides, SiMaN also merits in its easy implementation, where the median of absolute weights acts as the boundary between 0s and +1s to ensure the bit entropy maximization, while the angle alignment is also guaranteed, as analyzed in Sec. 4.3. In contrast, RBNN has to learn two complex rotation matrices and applies them in the beginning phase of each training epoch to reduce the angle bias.

5.5 Results on ImageNet

We also conduct similar experiments on ImageNet to validate the performance of SiMaN on a large-scale dataset. Two common networks, ResNet-18 and ResNet-34, are adopted

for binarization. Table 3 shows the results of SiMaN and several other binarization methods. The performance of SiMaN on ImageNet also takes the leading place. Specifically, with ResNet-18, SiMaN achieves 60.1% top-1 and 82.3% top-5 accuracies, respectively, with 0.2% and 0.4% improvements over RBNN. With ResNet-34, it achieves a top-1 accuracy of 63.9% and a top-5 accuracy of 84.8%, outperforming RBNN by 0.8% and 0.4%, respectively.

The performance improvements in Table 2 and Table 3 strongly demonstrate the impact of exploring discrete optimization and the effectiveness of our magnitude-based discrete solution in constructing a high-performing BNN.

6 CONCLUSION

In this paper, we proposed a novel sign-to-magnitude network binarization (SiMaN) scheme that avoids the dependency on the sign function, to optimize a binary neural network for higher accuracy. Our SiMaN reformulates the angle alignment between the weight vector and its binarization as being constrained to $\{0, +1\}$. We proved that an analytical discrete solution can be attained in a computationally efficient manner by encoding into +1s the high-magnitude weights, and 0s otherwise. We also mathematically proved that the learned weights roughly follow a Laplacian distribution, which is harmful to bit entropy maximization. To address the problem, we have shown that simply removing the ℓ_2 regularization during network training can break the Laplacian distribution and lead to a half-half distribution of binarized weights. As a result, the complexity of our binarization could be further simplified by encoding into +1 weights within the largest top-half magnitude, and 0 otherwise. Our experimental results demonstrate the significant performance improvement of SiMaN.

ACKNOWLEDGEMENT

This work is supported by the National Natural Science Foundation of China (No.U1705262, No.61772443, No.61572410, No.61802324 and No.61702136), National Key R&D Program (No.2017YFC0113000, and No.2016YFB1001503), Key R&D Program of Jiangxi Province (No. 20171ACH80022), Natural Science Foundation of Guangdong Province in China (No.2019B1515120049) and National Key R&D Plan Project (No.2018YFC0830105 and No.2018YFC0830100).

APPENDIX A

THE PRACTICAL PROPORTION OF +1S.

We further display more about the practical proportion of weights being encoded into +1s in different layers of different networks when trained with and without the ℓ_2 regularization to support our Corollary 2 that $w \in \mathbf{w}$ roughly follows a zero-mean Laplacian distribution.

From Figs. 5–13, we can see that, the proportion of +1s trained with ℓ_2 regularization, falls into the range between 0.36 and 0.38, which is very close to the theoretical result of 0.37 for the Laplacian distribution. Thus, the trained weights follow the Laplacian distribution. By removing the ℓ_2 regularization during network training, the proportion of +1s increases to the range between 0.50 and 0.52, which is very close to the ideal half-half distribution.

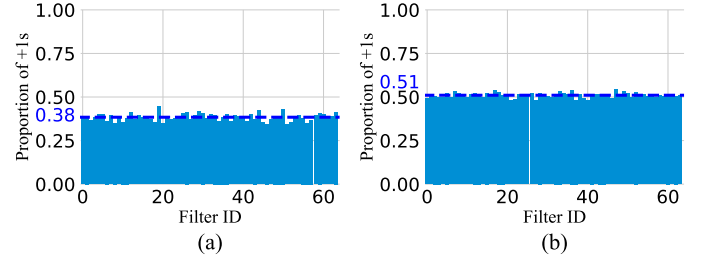


Fig. 5. Proportion of +1s trained (a) with and (b) without the ℓ_2 regularization (Layer1.1.2 of ResNet-18). The dashed blue lines denote the average proportions of +1s of all filter weights (Best view with zooming in).

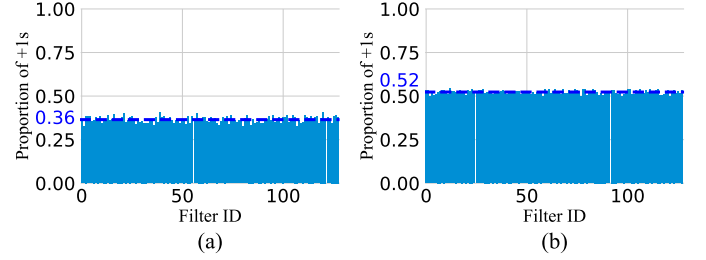


Fig. 6. Proportion of +1s trained (a) with and (b) without the ℓ_2 regularization (Layer2.1.2 of ResNet-18). The dashed blue lines denote the average proportions of +1s of all filter weights (Best view with zooming in).

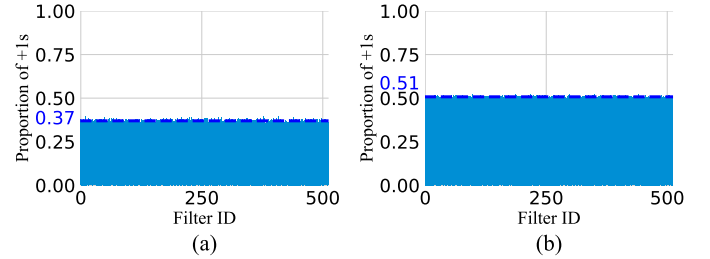


Fig. 7. Proportion of +1s trained (a) with and (b) without the ℓ_2 regularization (Layer4.1.2 of ResNet-18). The dashed blue lines denote the average proportions of +1s of all filter weights (Best view with zooming in).

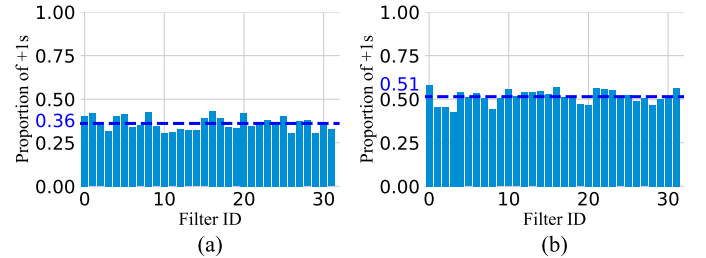


Fig. 8. Proportion of +1s trained (a) with and (b) without the ℓ_2 regularization (Layer2.1.2 of ResNet-20). The dashed blue lines denote the average proportions of +1s of all filter weights (Best view with zooming in).

REFERENCES

- [1] K. He, X. Zhang, S. Ren, and J. Sun, “Deep residual learning for image recognition,” in *Proceedings of the IEEE Conference on*

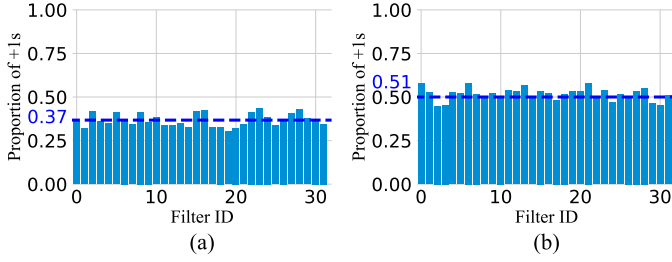


Fig. 9. Proportion of +1s trained (a) with and (b) without the ℓ_2 regularization (Layer2.2.2 of ResNet-20). The dashed blue lines denote the average proportions of +1s of all filter weights (Best view with zooming in).

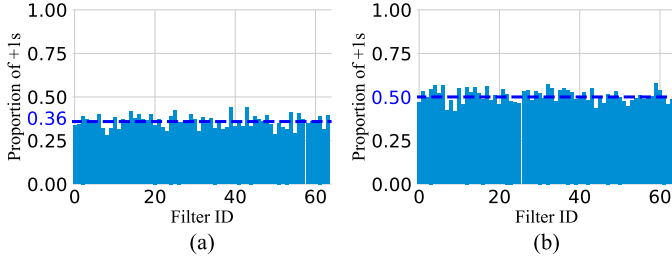


Fig. 10. Proportion of +1s trained (a) with and (b) without the ℓ_2 regularization (Layer3.2.1 of ResNet-20). The dashed blue lines denote the average proportions of +1s of all filter weights (Best view with zooming in).

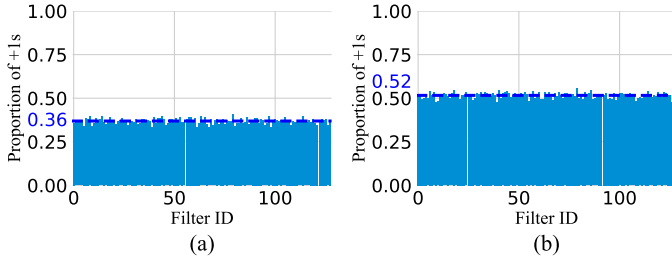


Fig. 11. Proportion of +1s trained (a) with and (b) without the ℓ_2 regularization (Layer1 of VGG). The dashed blue lines denote the average proportions of +1s of all filter weights (Best view with zooming in).

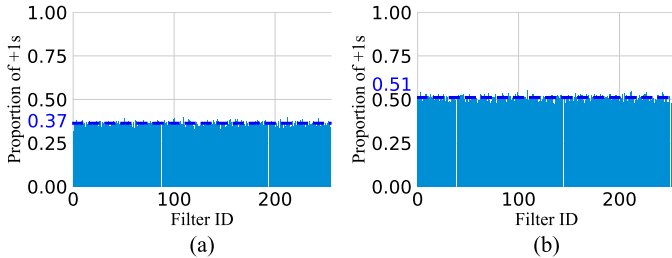


Fig. 12. Proportion of +1s trained (a) with and (b) without the ℓ_2 regularization (Layer2 of VGG). The dashed blue lines denote the average proportions of +1s of all filter weights (Best view with zooming in).

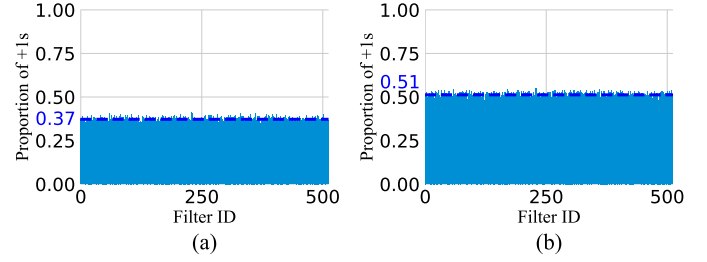


Fig. 13. Proportion of +1s trained (a) with and (b) without the ℓ_2 regularization (Layer4 of VGG). The dashed blue lines denote the average proportions of +1s of all filter weights (Best view with zooming in).

[2] Y. Wei, W. Xia, M. Lin, J. Huang, B. Ni, J. Dong, Y. Zhao, and S. Yan, "Hcp: A flexible cnn framework for multi-label image classification," *IEEE Transactions on Pattern Analysis and Machine Intelligence (T-PAMI)*, vol. 38, no. 9, pp. 1901–1907, 2015.

[3] K. He, X. Zhang, S. Ren, and J. Sun, "Spatial pyramid pooling in deep convolutional networks for visual recognition," *IEEE Transactions on Pattern Analysis and Machine Intelligence (T-PAMI)*, vol. 37, no. 9, pp. 1904–1916, 2015.

[4] J. Redmon, S. Divvala, R. Girshick, and A. Farhadi, "You only look once: Unified, real-time object detection," in *Proceedings of the IEEE Conference on Computer Vision and Pattern Recognition (CVPR)*, 2016, pp. 779–788.

[5] S. Ren, K. He, R. Girshick, X. Zhang, and J. Sun, "Object detection networks on convolutional feature maps," *IEEE Transactions on Pattern Analysis and Machine Intelligence (T-PAMI)*, vol. 39, no. 7, pp. 1476–1481, 2016.

[6] X. Zhang, F. Wan, C. Liu, X. Ji, and Q. Ye, "Learning to match anchors for visual object detection," *IEEE Transactions on Pattern Analysis and Machine Intelligence (T-PAMI)*.

[7] J. Long, E. Shelhamer, and T. Darrell, "Fully convolutional networks for semantic segmentation," in *Proceedings of the IEEE Conference on Computer Vision and Pattern Recognition (CVPR)*, 2015, pp. 3431–3440.

[8] V. Badrinarayanan, A. Kendall, and R. Cipolla, "Segnet: A deep convolutional encoder-decoder architecture for image segmentation," *IEEE Transactions on Pattern Analysis and Machine Intelligence (T-PAMI)*, vol. 39, no. 12, pp. 2481–2495, 2017.

[9] E. Shelhamer, J. Long, and T. Darrell, "Fully convolutional networks for semantic segmentation," *IEEE Transactions on Pattern Analysis and Machine Intelligence (T-PAMI)*, vol. 39, no. 4, pp. 640–651, 2017.

[10] S. Han, J. Pool, J. Tran, and W. Dally, "Learning both weights and connections for efficient neural network," in *Proceedings of the Advances in Neural Information Processing Systems (NeurIPS)*, 2015, pp. 1135–1143.

[11] J. Frankle and M. Carbin, "The lottery ticket hypothesis: Finding sparse, trainable neural networks," in *Proceedings of the International Conference on Learning Representations (ICLR)*, 2019.

[12] J.-H. Luo, H. Zhang, H.-Y. Zhou, C.-W. Xie, J. Wu, and W. Lin, "Thinet: pruning cnn filters for a thinner net," *IEEE Transactions on Pattern Analysis and Machine Intelligence (T-PAMI)*, vol. 41, no. 10, pp. 2525–2538, 2018.

[13] M. Lin, R. Ji, Y. Wang, Y. Zhang, B. Zhang, Y. Tian, and L. Shao, "Hrank: Filter pruning using high-rank feature map," in *Proceedings of the IEEE Conference on Computer Vision and Pattern Recognition (CVPR)*, 2020, pp. 1529–1538.

[14] X. Zhang, X. Zhou, M. Lin, and J. Sun, "Shufflenet: An extremely efficient convolutional neural network for mobile devices," in *Proceedings of the IEEE Conference on Computer Vision and Pattern Recognition (CVPR)*, 2018, pp. 6848–6856.

[15] N. Ma, X. Zhang, H.-T. Zheng, and J. Sun, "Shufflenet v2: Practical guidelines for efficient cnn architecture design," in *Proceedings of the European Conference on Computer Vision (ECCV)*, 2018, pp. 116–131.

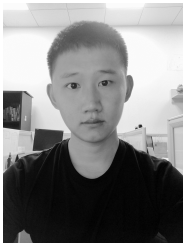
[16] A. G. Howard, M. Zhu, B. Chen, D. Kalenichenko, W. Wang, T. Weyand, M. Andreetto, and H. Adam, "Mobilenets: Efficient convolutional neural networks for mobile vision applications," *arXiv preprint arXiv:1704.04861*, 2017.

[17] M. Sandler, A. Howard, M. Zhu, A. Zhmoginov, and L.-C. Chen, "Mobilenetv2: Inverted residuals and linear bottlenecks," in *Proceedings of the IEEE Conference on Computer Vision and Pattern Recognition (CVPR)*, 2018, pp. 4510–4520.

- [18] A. Howard, M. Sandler, G. Chu, L.-C. Chen, B. Chen, M. Tan, W. Wang, Y. Zhu, R. Pang, V. Vasudevan *et al.*, "Searching for mobilenetv3," in *Proceedings of the IEEE Conference on Computer Vision and Pattern Recognition (CVPR)*, 2019, pp. 1314–1324.
- [19] K. Han, Y. Wang, Q. Tian, J. Guo, C. Xu, and C. Xu, "Ghostnet: More features from cheap operations," in *Proceedings of the IEEE Conference on Computer Vision and Pattern Recognition (CVPR)*, 2020, pp. 1580–1589.
- [20] S. Lin, R. Ji, C. Chen, D. Tao, and J. Luo, "Holistic crn compression via low-rank decomposition with knowledge transfer," *IEEE Transactions on Pattern Analysis and Machine Intelligence (T-PAMI)*, vol. 41, no. 12, pp. 2889–2905, 2018.
- [21] K. Hayashi, T. Yamaguchi, Y. Sugawara, and S.-i. Maeda, "Exploring unexplored tensor network decompositions for convolutional neural networks," in *Proceedings of the Advances in Neural Information Processing Systems (NeurIPS)*, 2019, pp. 5552–5562.
- [22] Z. Cai, X. He, J. Sun, and N. Vasconcelos, "Deep learning with low precision by half-wave gaussian quantization," in *Proceedings of the IEEE Conference on Computer Vision and Pattern Recognition (CVPR)*, 2017, pp. 5918–5926.
- [23] K. Han, Y. Wang, Y. Xu, C. Xu, E. Wu, and C. Xu, "Training binary neural networks through learning with noisy supervision," in *Proceedings of the International Conference on Machine Learning (ICML)*, 2020, pp. 4017–4026.
- [24] M. Lin, R. Ji, Z. Xu, B. Zhang, Y. Wang, Y. Wu, F. Huang, and C.-W. Lin, "Rotated binary neural network," in *Proceedings of the Advances in Neural Information Processing Systems (NeurIPS)*, 2020.
- [25] M. Rastegari, V. Ordonez, J. Redmon, and A. Farhadi, "Xnor-net: Imagenet classification using binary convolutional neural networks," in *Proceedings of the European Conference on Computer Vision (ECCV)*, 2016, pp. 525–542.
- [26] J. Deng, W. Dong, R. Socher, L.-J. Li, K. Li, and L. Fei-Fei, "Imagenet: A large-scale hierarchical image database," in *Proceedings of the IEEE Conference on Computer Vision and Pattern Recognition (CVPR)*, 2009, pp. 248–255.
- [27] X. Lin, C. Zhao, and W. Pan, "Towards accurate binary convolutional neural network," in *Proceedings of the Advances in Neural Information Processing Systems (NeurIPS)*, 2017, pp. 345–353.
- [28] Z. Liu, B. Wu, W. Luo, X. Yang, W. Liu, and K.-T. Cheng, "Bi-real net: Enhancing the performance of 1-bit cnns with improved representational capability and advanced training algorithm," in *Proceedings of the European Conference on Computer Vision (ECCV)*, 2018, pp. 722–737.
- [29] H. Qin, R. Gong, X. Liu, M. Shen, Z. Wei, F. Yu, and J. Song, "Forward and backward information retention for accurate binary neural networks," in *Proceedings of the IEEE Conference on Computer Vision and Pattern Recognition (CVPR)*, 2020, pp. 2250–2259.
- [30] J. Gu, J. Zhao, X. Jiang, B. Zhang, J. Liu, G. Guo, and R. Ji, "Bayesian optimized 1-bit cnns," in *Proceedings of the IEEE International Conference on Computer Vision (ICCV)*, 2019, pp. 4909–4917.
- [31] M. Courbariaux, Y. Bengio, and J.-P. David, "Binaryconnect: Training deep neural networks with binary weights during propagations," in *Proceedings of the Advances in Neural Information Processing Systems (NeurIPS)*, 2015, pp. 3123–3131.
- [32] M. Courbariaux, I. Hubara, D. Soudry, R. El-Yaniv, and Y. Bengio, "Binarized neural networks: Training deep neural networks with weights and activations constrained to+ 1 or-1," *arXiv preprint arXiv:1602.02830*, 2016.
- [33] A. Krizhevsky, G. Hinton *et al.*, "Learning multiple layers of features from tiny images," 2009.
- [34] Y. Bengio, N. Léonard, and A. Courville, "Estimating or propagating gradients through stochastic neurons for conditional computation," *arXiv preprint arXiv:1308.3432*, 2013.
- [35] T. Simons and D.-J. Lee, "A review of binarized neural networks," *Electronics*, vol. 8, no. 6, p. 661, 2019.
- [36] H. Qin, R. Gong, X. Liu, X. Bai, J. Song, and N. Sebe, "Binary neural networks: A survey," *Pattern Recognition (PR)*, vol. 105, p. 107281, 2020.
- [37] A. Bulat and G. Tzimiropoulos, "Xnor-net++: Improved binary neural networks," in *Proceedings of the British Machine Vision Conference (BMVC)*, 2019.
- [38] S. Darabi, M. Belbahri, M. Courbariaux, and V. P. Nia, "Bnn+: Improved binary network training," *arXiv preprint arXiv:1812.11800*, 2018.
- [39] J. W. Peters and M. Welling, "Probabilistic binary neural networks," *arXiv preprint arXiv:1809.03368*, 2018.
- [40] O. Shayer, D. Levi, and E. Fetaya, "Learning discrete weights using the local reparameterization trick," in *Proceedings of the International Conference on Learning Representations (ICLR)*, 2018.
- [41] C. Leng, Z. Dou, H. Li, S. Zhu, and R. Jin, "Extremely low bit neural network: Squeeze the last bit out with admm," in *Proceedings of the AAAI Conference on Artificial Intelligence (AAAI)*, 2018.
- [42] M. Alizadeh, J. Fernández-Marqués, N. D. Lane, and Y. Gal, "An empirical study of binary neural networks' optimisation," in *Proceedings of the International Conference on Learning Representations (ICLR)*, 2018.
- [43] J. Bethge, H. Yang, M. Bornstein, and C. Meinel, "Back to simplicity: How to train accurate bnns from scratch?" *arXiv preprint arXiv:1906.08637*, 2019.
- [44] K. Helwegen, J. Widdicombe, L. Geiger, Z. Liu, K.-T. Cheng, and R. Nusselder, "Latent weights do not exist: Rethinking binarized neural network optimization," in *Proceedings of the Advances in Neural Information Processing Systems (NeurIPS)*, 2019, pp. 7533–7544.
- [45] B. Martinez, J. Yang, A. Bulat, and G. Tzimiropoulos, "Training binary neural networks with real-to-binary convolutions," in *International Conference on Learning Representations (ICLR)*, 2019.
- [46] A. G. Anderson and C. P. Berg, "The high-dimensional geometry of binary neural networks," in *International Conference on Learning Representations (ICLR)*, 2018.
- [47] J. Gu, C. Li, B. Zhang, J. Han, X. Cao, J. Liu, and D. Doermann, "Projection convolutional neural networks for 1-bit cnns via discrete back propagation," in *Proceedings of the AAAI Conference on Artificial Intelligence (AAAI)*, 2019, pp. 8344–8351.
- [48] R. Ding, T.-W. Chin, Z. Liu, and D. Marculescu, "Regularizing activation distribution for training binarized deep networks," in *Proceedings of the IEEE Conference on Computer Vision and Pattern Recognition (CVPR)*, 2019, pp. 11 408–11 417.
- [49] Z. Liu, Z. Shen, M. Savvides, and K.-T. Cheng, "Reactnet: Towards precise binary neural network with generalized activation functions," in *Proceedings of the European Conference on Computer Vision (ECCV)*, 2020, pp. 143–159.
- [50] I. Hubara, M. Courbariaux, D. Soudry, R. El-Yaniv, and Y. Bengio, "Binarized neural networks," in *Proceedings of the Advances in Neural Information Processing Systems (NeurIPS)*, 2016, pp. 4107–4115.
- [51] S. Zhou, Y. Wu, Z. Ni, X. Zhou, H. Wen, and Y. Zou, "Dorefa-net: Training low bitwidth convolutional neural networks with low bitwidth gradients," *arXiv preprint arXiv:1606.06160*, 2016.
- [52] M. Conforti, G. Cornuéjols, G. Zambelli *et al.*, *Integer programming*, 2014, vol. 271.
- [53] R. Banner, Y. Nahshan, E. Hoffer, and D. Soudry, "Post-training 4-bit quantization of convolution networks for rapid-deployment," *arXiv preprint arXiv:1810.05723*, 2018.
- [54] K. Zhong, T. Zhao, X. Ning, S. Zeng, K. Guo, Y. Wang, and H. Yang, "Towards lower bit multiplication for convolutional neural network training," *arXiv preprint arXiv:2006.02804*, 2020.
- [55] C. M. Shakarji and V. Srinivasan, "Theory and algorithms for weighted total least-squares fitting of lines, planes, and parallel planes to support tolerancing standards," *Journal of Computing and Information Science in Engineering*, vol. 13, no. 3, 2013.
- [56] D. Wan, F. Shen, L. Liu, F. Zhu, J. Qin, L. Shao, and H. Tao Shen, "Tbn: Convolutional neural network with ternary inputs and binary weights," in *Proceedings of the European Conference on Computer Vision (ECCV)*, 2018, pp. 315–332.
- [57] R. Gong, X. Liu, S. Jiang, T. Li, P. Hu, J. Lin, F. Yu, and J. Yan, "Differentiable soft quantization: Bridging full-precision and low-bit neural networks," in *Proceedings of the IEEE International Conference on Computer Vision (ICCV)*, 2019, pp. 4852–4861.
- [58] Z. Yang, Y. Wang, K. Han, C. Xu, C. Xu, D. Tao, and C. Xu, "Searching for low-bit weights in quantized neural networks," in *Proceedings of the Advances in Neural Information Processing Systems (NeurIPS)*, 2020.
- [59] P. Wang, X. He, G. Li, T. Zhao, and J. Cheng, "Sparsity-inducing binarized neural networks," in *Proceedings of the AAAI Conference on Artificial Intelligence (AAAI)*, 2020, pp. 12 192–12 199.
- [60] D. Zhang, J. Yang, D. Ye, and G. Hua, "Lq-nets: Learned quantization for highly accurate and compact deep neural networks," in *Proceedings of the European Conference on Computer Vision (ECCV)*, 2018, pp. 365–382.
- [61] A. Paszke, S. Gross, F. Massa, A. Lerer, J. Bradbury, G. Chanan, T. Killeen, Z. Lin, N. Gimelshein, L. Antiga *et al.*, "Pytorch:

An imperative style, high-performance deep learning library," in *Proceedings of the Advances in Neural Information Processing Systems (NeurIPS)*, 2019, pp. 8026–8037.

- [62] L. Hou, Q. Yao, and J. T. Kwok, "Loss-aware binarization of deep networks," in *Proceedings of the International Conference on Learning Representations (ICLR)*, 2016.
- [63] Z. Wang, J. Lu, C. Tao, J. Zhou, and Q. Tian, "Learning channel-wise interactions for binary convolutional neural networks," in *Proceedings of the IEEE Conference on Computer Vision and Pattern Recognition (CVPR)*, 2019, pp. 568–577.
- [64] J. Bethge, C. Bartz, H. Yang, Y. Chen, and C. Meinel, "Meliusnet: Can binary neural networks achieve mobilenet-level accuracy?" *arXiv preprint arXiv:2001.05936*, 2020.
- [65] S. Zhu, X. Dong, and H. Su, "Binary ensemble neural network: More bits per network or more networks per bit?" in *Proceedings of the IEEE Conference on Computer Vision and Pattern Recognition (CVPR)*, 2019, pp. 4923–4932.



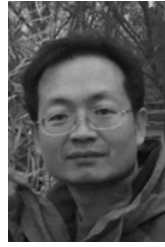
Mingbao Lin is currently pursuing the Ph.D degree with Xiamen University, China. He has published over ten papers as the first author in international journals and conferences, including IEEE TPAMI, IJCV, IEEE TIP, IEEE TNNLS, CVPR, NeurIPS, AAAI, IJCAI, ACM MM and so on. His current research interest includes network compression & acceleration, and information retrieval.



Rongrong Ji (Senior Member, IEEE) is currently a Professor and the Director of the Intelligent Multimedia Technology Laboratory, and the Dean Assistant with the School of Information Science and Engineering, Xiamen University, Xiamen, China. His work mainly focuses on innovative technologies for multimedia signal processing, computer vision, and pattern recognition, with over 100 papers published in international journals and conferences. He is a member of the ACM. He was a recipient of the ACM Multimedia Best Paper Award and the Best Thesis Award of Harbin Institute of Technology. He serves as an Associate/Guest Editor for international journals and magazines such as *Neurocomputing*, *Signal Processing*, *Multimedia Tools and Applications*, the *IEEE Multimedia Magazine*, and the *Multimedia Systems*. He also serves as program committee member for several Tier-1 international conferences.

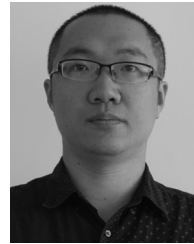


Zihan Xu received the B.S. degree in applied mathematics from Zhengzhou University, China, in 2019. He is currently pursuing the M.S. degree with Xiamen University, China. His research interests include computer vision and machine learning.



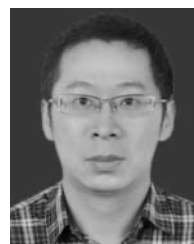
face recognition, and wavelets.

Baochang Zhang (Senior Member, IEEE) received the B.S., M.S., and Ph.D. degrees in computer science from the Harbin Institute of Technology, Harbin, China, in 1999, 2001, and 2006, respectively. From 2006 to 2008, he was a Research Fellow with The Chinese University of Hong Kong, Hong Kong, and also with Griffith University, Brisbane, Australia. He is currently a full Professor with Beihang University, Beijing, China. His current research interests include pattern recognition, machine learning,



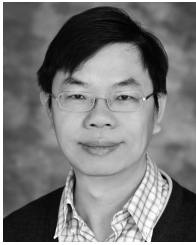
Fei Chao (Member, IEEE) received the B.Sc. degree in mechanical engineering from the Fuzhou University, Fuzhou, China, in 2004, the M.Sc. degree with distinction in computer science from the University of Wales, Aberystwyth, U.K., in 2005, and the Ph.D. degree in robotics from the Aberystwyth University, Wales, U.K., in 2009.

He is currently an Associate Professor with the School of Informatics, Xiamen University, Xiamen, China. He has authored/co-authored more than 50 peer-reviewed journal and conference papers. His current research interests include developmental robotics, machine learning, and optimization algorithms.



artificial intelligence.

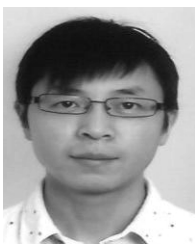
Mingliang Xu received the Ph.D. degree in computer science and technology from the State Key Lab of CAD and CG, Zhejiang University, Hangzhou, China, in 2011. He is currently a Full Professor with the School of Information Engineering, Zhengzhou University, Zhengzhou, China, where he is currently the Director of the Center for Interdisciplinary Information Science Research and the Vice General Secretary of ACM SIGAI China. His current research interests include computer graphics, multimedia, and



Chia-Wen Lin (Fellow, IEEE) received the Ph.D degree in electrical engineering from National Tsing Hua University (NTHU), Hsinchu, Taiwan, in 2000. He is currently Professor with the Department of Electrical Engineering and the Institute of Communications Engineering, NTHU. He is also Deputy Director of the AI Research Center of NTHU. He was with the Department of Computer Science and Information Engineering, National Chung Cheng University, Taiwan, during 2000–2007. Prior to joining academia, he

worked for the Information and Communications Research Laboratories, Industrial Technology Research Institute, Hsinchu, Taiwan, during 1992–2000. His research interests include image and video processing, computer vision, and video networking.

Dr. Lin served as Distinguished Lecturer of IEEE Circuits and Systems Society from 2018 to 2019, a Steering Committee member of IEEE TRANSACTIONS ON MULTIMEDIA from 2014 to 2015, and the Chair of the Multimedia Systems and Applications Technical Committee of the IEEE Circuits and Systems Society from 2013 to 2015. His articles received the Best Paper Award of IEEE VCIP 2015 and the Young Investigator Award of VCIP 2005. He received Outstanding Electrical Professor Award presented by Chinese Institute of Electrical Engineering in 2019, and Young Investigator Award presented by Ministry of Science and Technology, Taiwan, in 2006. He is also the Chair of the Steering Committee of IEEE ICME. He has served as a Technical Program Co-Chair for IEEE ICME 2010, and a General Co-Chair for IEEE VCIP 2018, and a Technical Program Co-Chair for IEEE ICIP 2019. He has served as an Associate Editor of IEEE TRANSACTIONS ON IMAGE PROCESSING, IEEE TRANSACTIONS ON CIRCUITS AND SYSTEMS FOR VIDEO TECHNOLOGY, IEEE TRANSACTIONS ON MULTIMEDIA, IEEE MULTIMEDIA, and *Journal of Visual Communication and Image Representation*.



Ling Shao (Fellow, IEEE) is currently the Executive Vice President and a Provost of the Mohamed bin Zayed University of Artificial Intelligence. He is also the CEO and the Chief Scientist of the Inception Institute of Artificial Intelligence (IIAI), Abu Dhabi, United Arab Emirates. His research interests include computer vision, machine learning, and medical imaging. He is a fellow of IEEE, IAPR, IET, and BCS.